<div align="center">

Supplemental information

for

</div>

Constructing a Highly Permeable Bioinspired Rigid-Flexible Coupled Membrane with a High Content of Spindle-Type MOF Integration: Efficient Adsorption Separation of Water-Soluble Pollutants

Ruilong Zhang[a,b], Jun Zhao[b,c*], Xiaohua Tian[a], Jian Ye[a], Lulu Wang[a], Ifunanya Rejoice Akaniro[b], Jianming Pan[a*], Jiangdong Dai[a*]

[a] Institute of Green Chemistry and Chemical Technology, Advanced Chemical Engineering Laboratory of Green Materials and Energy of Jiangsu Province, School of Chemistry and Chemical Engineering, Jiangsu University, Zhenjiang, China

[b] Department of Biology, Institute of Bioresource and Agriculture, Hong Kong Baptist University, Kowloon Tong, Hong Kong Special Administrative Region of China

[c] Institute of Advanced Materials, Hong Kong Baptist University, Kowloon Tong, Hong Kong Special Administrative Region of China

* Corresponding author: zhaojun@hkbu.edu.hk (Jun Zhao); pjm@ujs.edu.cn (Jianming Pan); daijd@ujs.edu.cn (Jiangdong Dai)

2. Experimental

2.1 Materials and chemicals

The PVDF membranes utilized in this investigation (with an average pore size of 0.22 μm) were sourced from Shanghai Xingya Purification Material Factory. Chemicals, such as ferric nitrate nonahydrate ($Fe(NO_3)_3 \cdot 9H_2O$), cobalt nitrate hexahydrate ($Co(NO_3)_2 \cdot 6H_2O$), N, N-dimethylformamide (DMF), fumaric acid (FA), methanol (MA), tannic acid (TA), methylene blue (MB), acid fuchsin (AF), methyl violet (MV-10B), amaranth, ponceau (PS), rhodamine B (RhB), methyl orange (MO), tetracycline (TC), tert-butyl alcohol (TBA), p-benzoquinone (P-BQ), furfuryl alcohol (FFA), and potassium peroxysulfate (PMS), were procured from Aladdin Reagent Co. LTD.

<div align="center">

Table S1 Name of prepared composite membranes

</div>

Sample	CoFe-MOF (mg L^{-1})	GO-TA (mg L^{-1})	CoFe-MOF proportion (%)
CoFe-MOF/GO-TA-0	50	0	100
CoFe-MOF/GO-TA-2	50	2	96.15
CoFe-MOF/GO-TA-5	50	5	90.91
CoFe-MOF/GO-TA-10	50	10	83.33
CoFe-MOF/GO-TA-15	50	15	76.92
CoFe-MOF/GO-TA-20	50	20	71.43

2.2 Characterization

The surface morphological features and elemental composition of the substances were scrutinized employing scanning electron microscopy (SEM, JSM-7800F, Japan) and energy dispersive X-ray spectroscopy (EDS). The molecular configuration of the materials was elucidated through attenuated total reflectance Fourier transform infrared spectroscopy (FTIR) (Nicolet NEXUS-470, America). The zeta potential and particle dimensions were ascertained utilizing a Zeta Potential and Particle Size Analyzer (Nano-zs90, England). The optical absorbance characteristics were quantified via a UV spectrophotometer (UV-2600, Japan). The internal microstructure of the materials was inspected using a thermal emission transmission electron microscope (TEM2100F, Japan), and their surface area was calculated using the Brunauer-Emmett-Teller (BET) method (NDVA-2000e, America). The fluorescence properties of the substances were investigated utilizing a fluorescence spectrophotometer (F98, China). The elemental composition and chemical state were probed employing X-ray photoelectron spectroscopy (AXIS ULTRA DLD, Japan) and X-ray diffractometry (XRD-6100Lab, Japan), respectively. Magnetic properties were assessed using an electron paramagnetic resonance spectrometer (JES-FA200, Japan). The degradation intermediate of RhB was analyzed by LC-MS (Thermo LXQ LC/MS, America). Electronic Universal Testing Machine

(DDL100) was used to determine the tensile strength.

3 Results and discussion

3.1 Catalyst characterization

FTIR analysis (**Fig.S4a**) was conducted on the functional group species of GO, GO-TA, CoFe-MOF, and CoFe-MOF/GO-TA. As depicted in Fig. 6a, the peaks at 3200-3700 cm^{-1} represented the O-H stretching vibrations, while the peak at 1708 cm^{-1} corresponded to the C=O vibration in the carboxyl group. All three samples (GO, GO-TA, and CoFe-MOF/GO-TA) exhibited distinct C=O functional groups, primarily attributed to the carboxyl groups on the surface of GO and the carboxyl groups of FA. The FTIR spectrum of CoFe-MOF displayed a peak at 1386 cm^{-1}, corresponding to the carboxyl group's asymmetric vibration in the FA molecule. The O-H bending vibration peak of H_2O was observed at 1620 cm^{-1}, more prominent in GO, indicating a higher content of water of crystallization in GO. The peak shifted to the right after modification by TA, attributed to the influence of hydroxyl groups on TA molecules. CoFe-MOF, on the other hand, exhibited no infrared absorption at 1620 cm^{-1}, indicating an absence of crystal water in its structure. Weak peaks at 946 cm^{-1} and 547 cm^{-1} in the FTIR spectrum of CoFe-MOF corresponded to the stretching vibration peaks of M-O/M-OH, consistent with literature reports, confirming the successful preparation of CoFe-MOF[1]. The absorption peak of CoFe-MOF/GO-TA resembled that of GO-TA, and a weak stretching vibration peak of M-O/M-OH appeared simultaneously, confirming the successful recombination of CoFe-MOF and GO-TA. In the stress-strain curves (**Fig.S4b**), a notable elevation in tensile stress was observed upon the deposition of CoFe-MOF and GO-TA onto the base membrane surface, predominantly ascribed to "brick and mortar" structure of CoFe-MOF/GO-TA. Conversely, a substantial decreased in strain was noted, potentially stemming from the vertical pressure exerted by the base film during the film deposition process, consequently impacting the transverse strain elasticity.
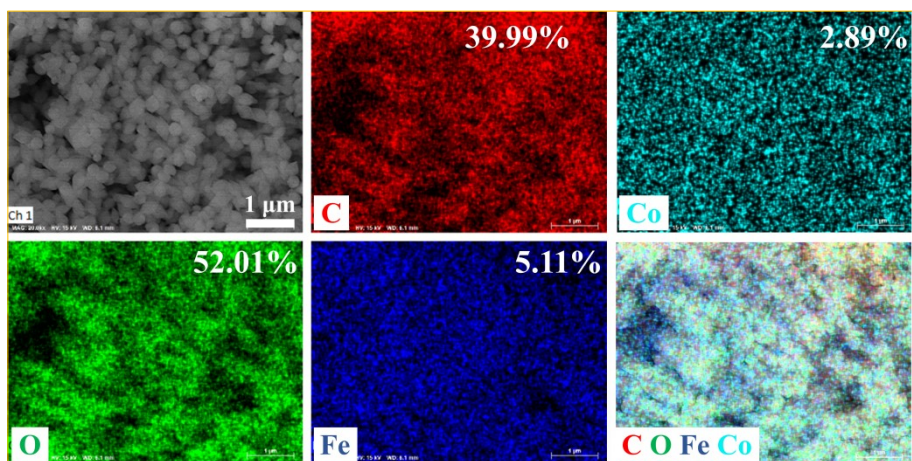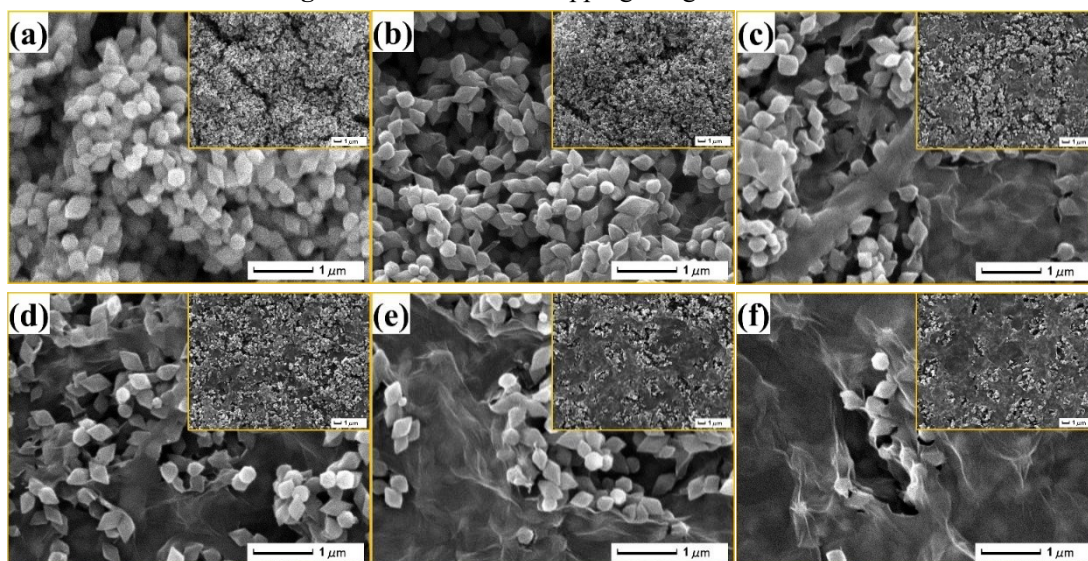
Fig.S1 SEM and EDS-Mapping images of CoFe-MOF

Fig.S2 Effect of GO-TA concentration on surface morphology of CoFe-MOF/GO-TA (0, 2.0, 5.0, 10.0, 15.0, and 20.0 mg L^{-1}) (a, b, c, d, e, and f)
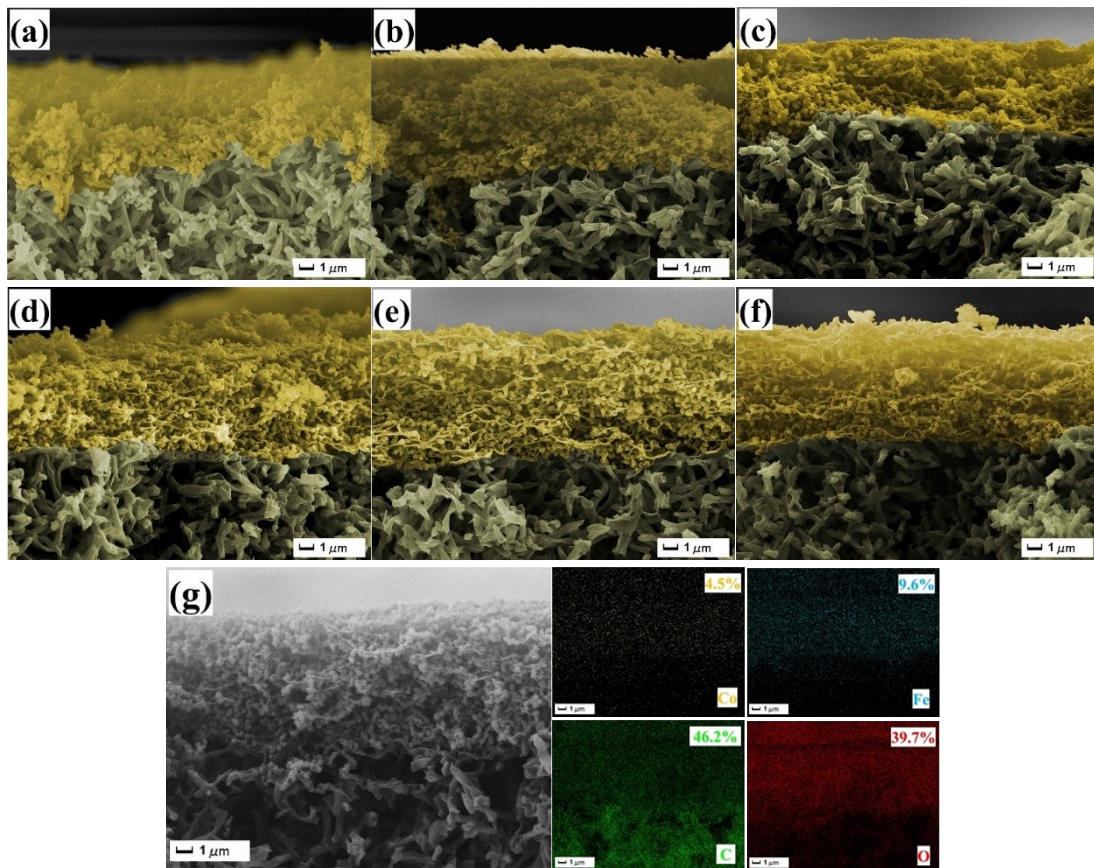
Fig.S3 Effect of GO-TA concentration on cross-section SEM image of CoFe-MOF/GO-TA (0, 2.0, 5.0, 10.0, 15.0, and 20.0 mg L^{-1}) (a, b, c, d, e, and f), and the EDS-Mapping image of CoFe-MOF/GO-TA-10 (g)
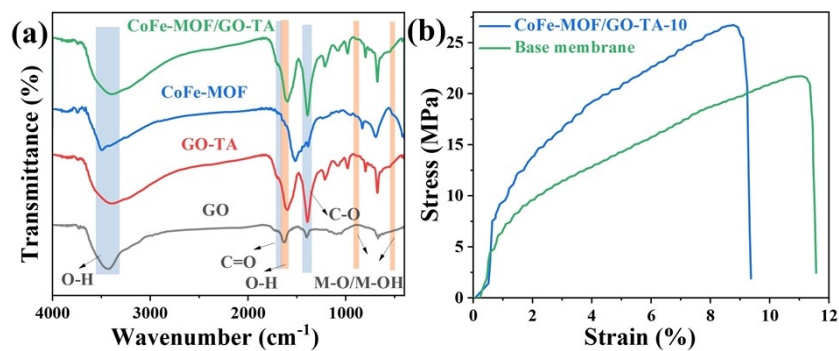
Fig.S4 FTIR of spectra (a), and the stress-train carves of base membrane and CoFe-MOF/GO-TA-10 (b)
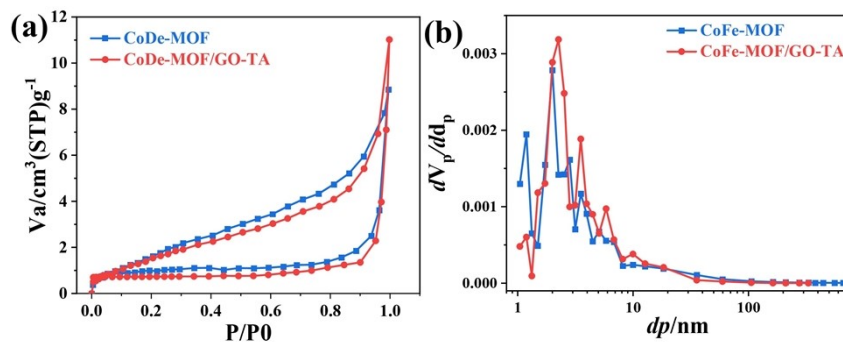
Fig.S5 N_2 adsorption-desorption curves (a) and pore size distribution (BJH method) (b) of CoFe-MOF and CoFe-MOF/GO-TA (powder)

Table.S2 Pore structure parameters of of CoFe-MOF and CoFe-MOF/GO-TA (powder)

Sample	V_m (cm^3 g^{-1})	S_{BET} (m^2 g^{-1})	D_{aver} (nm)
CoFe-MOF	1.84	8.03	5.67
CoFe-MOF/GO-TA	1.5658	6.81	9.249
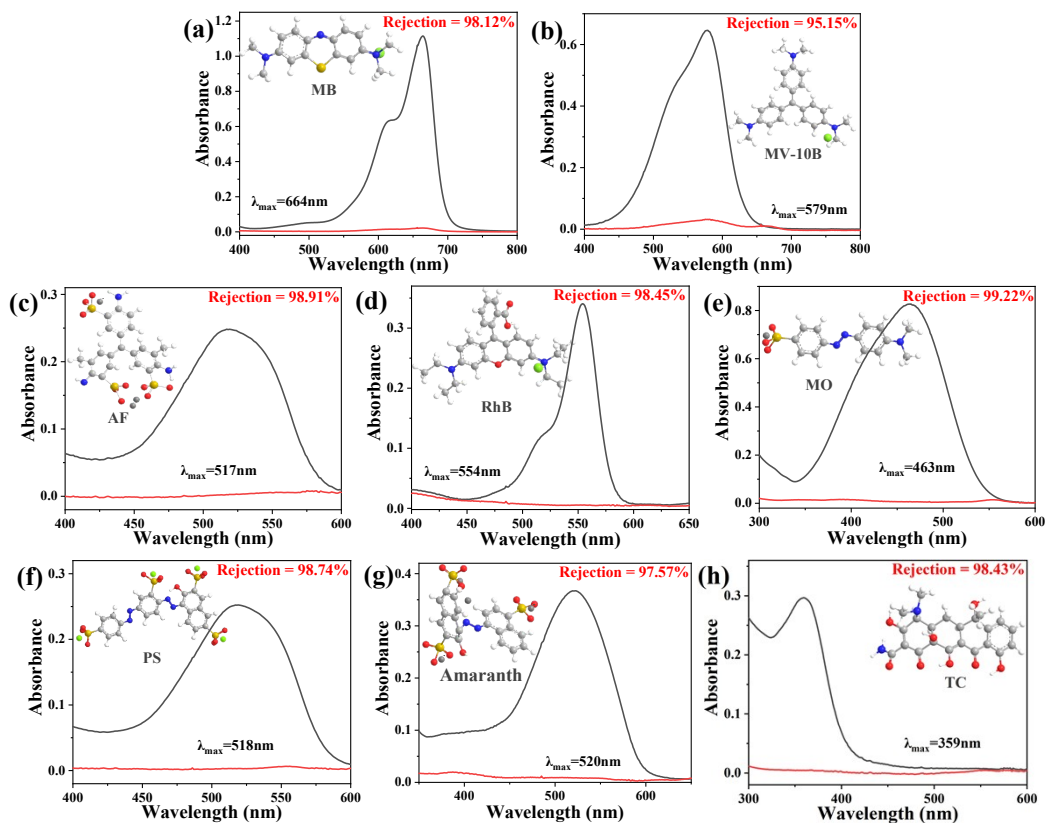
Fig.S6 UV absorption spectra of initial solution and filtrate of different pollutant solution reported by literatures
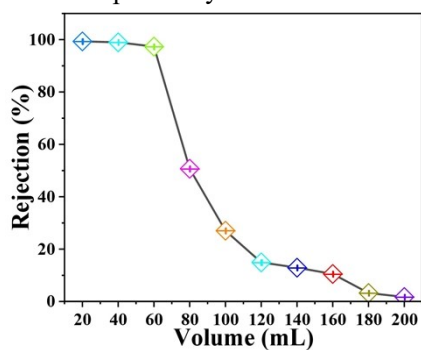
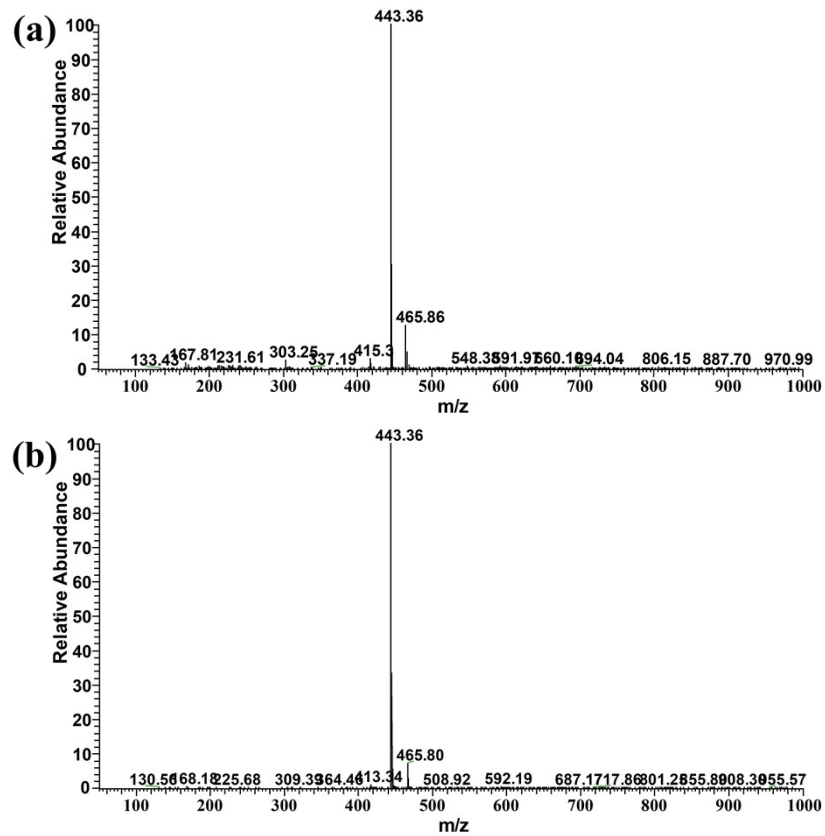**Fig.S7** Rejection of every 20 ml in the dynamic adsorption process for RhB

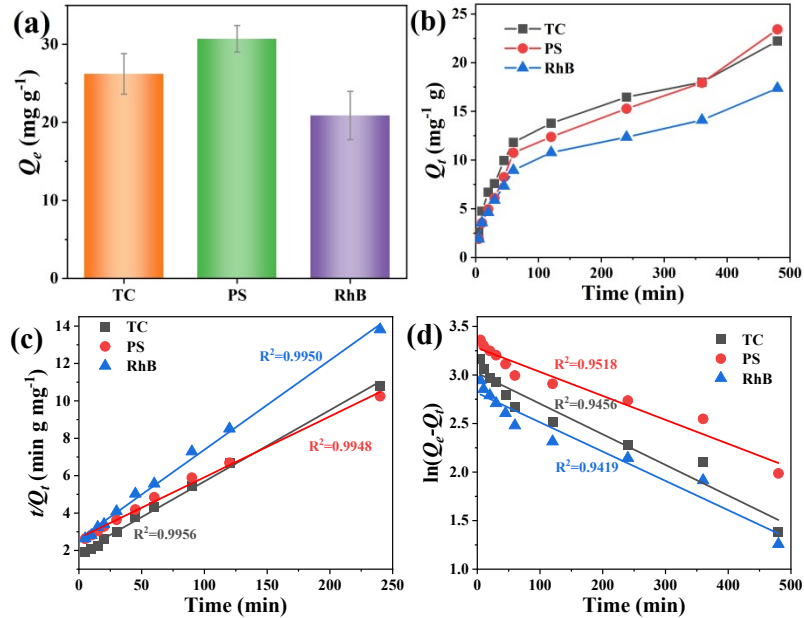**Fig.S8** Mass spectrum of RhB before filtration (a) and after filtration (b) using CoFe-MOF/GO-TA-10

Fig.S9 Adsorption capacity (a), kinetic curves (b), quasi-second-order kinetic (c), and quasi-first-order (d) of diffusion model of different pollutants for CoFe-MOF
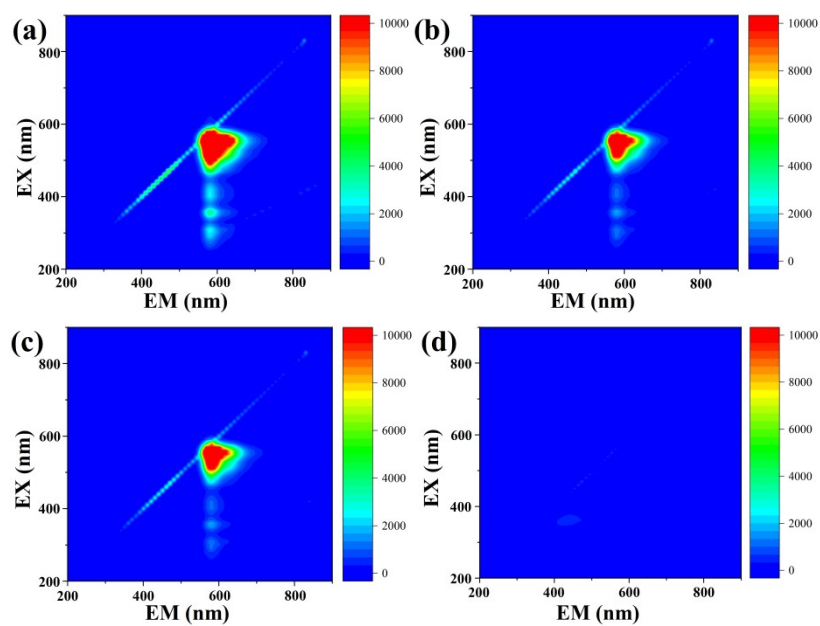
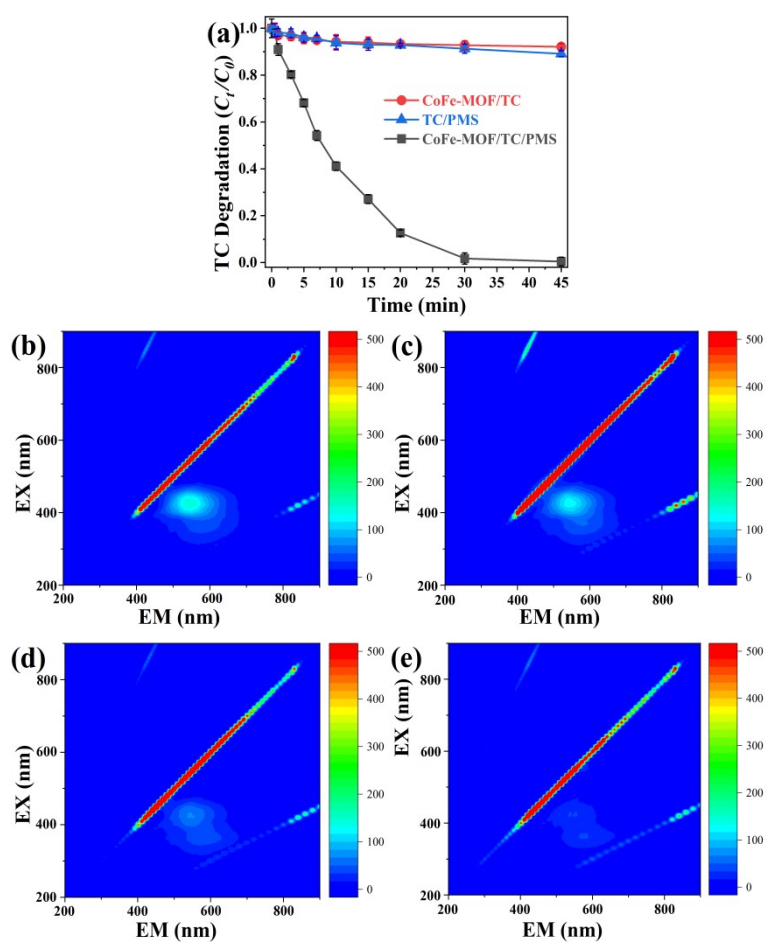**Fig.S10** 3D EEMs of RhB after degradation for 0 min (a), 3 min (b), 8 min (c), and 16 min (d)

Fig.S11 Process (a) and 3D EEMs of TC of degradation for 0 min (b), 5 min (c), 10 min (d), and 30 min (e). Condition: [Catalyst] = 20 mg L^{-1}, [RhB] = 20 mg L^{-1}, [PMS] = 100 mg L^{-1}
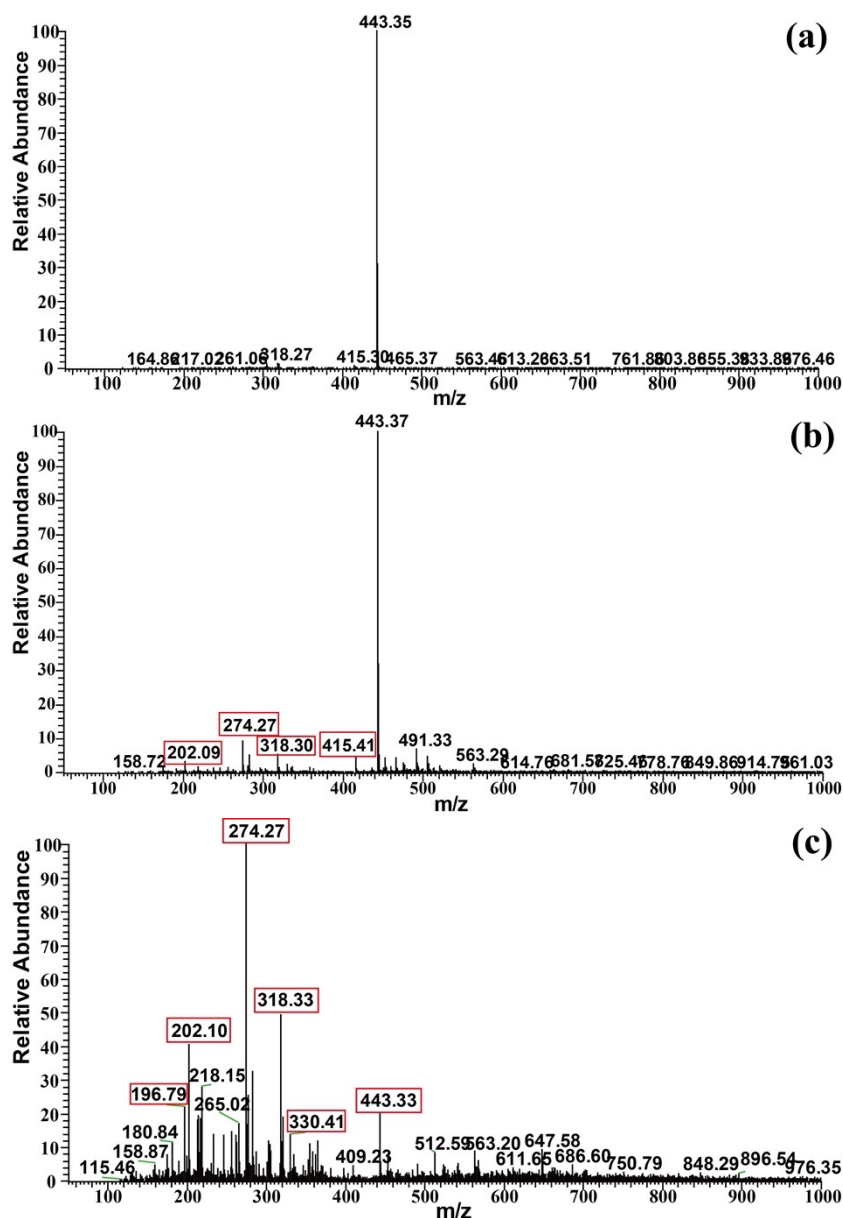
Fig.S12 Mass spectrum of RhB at different reaction time in CoFe-MOF/PMS system, 0 min (a), 1 min (b), and 10 min (c)
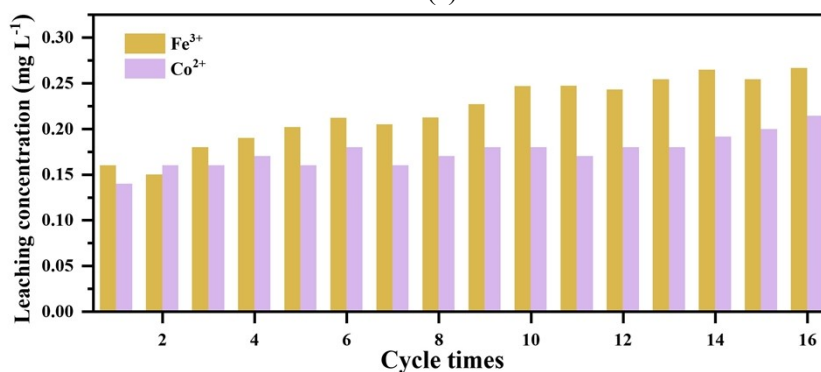

Fig.S13 Leaching ion concentration in the cyclic separation performance of CoFe-MOF/GO-TA-10 for RhB

[1] M. Safari, J. Mazloom, Electrochemical performance of spindle-like Fe_2Co-MOF and derived magnetic yolk-shell $CoFe_2O_4$ microspheres for supercapacitor applications, Journal of Solid State Electrochemistry, 25 (2021) 2189-2200.